Low Temperature Techniques for Natural Gas Purification and LNG Production: an Energy and Exergy Analysis

Margaret Baccanelli[a], Stefano Langé[a], Matteo V. Rocco[b], Laura A. Pellegrini[a], Emanuela Colombo[b]*

[a]Politecnico di Milano, Dipartimento di Chimica, Materiali e Ingegneria Chimica "G. Natta", Politecnico di Milano, Piazza Leonardo da Vinci 32, I-20133 Milano, Italy

[b]Politecnico di Milano, Dipartimento di Energia, via Lambruschini 4, Milan, Italy

E-mail addresses: margaret.baccanelli@mail.polimi.it; stefano.lange@polimi.it; matteovincenzo.rocco@polimi.it; laura.pellegrini@polimi.it; emanuela.colombo@polimi.it

Corresponding author: Stefano Langé; stefano.lange@polimi.it; Tel.: +390223994704

Abstract

Due to the rapid increase of the World's primary energy demand of the last decades, low-temperature processes for the purification of natural gas streams with high carbon dioxide content has gained interest, since they allow to make profitable exploitation of low-quality gas reserves. Low temperature purification processes allow the direct production of a methane stream at high purity and at low-temperature, suitable conditions for the direct synergistic integration with natural gas cryogenic liquefaction processes, while CO_2 is obtained in liquid phase and under pressure. In this way, it can be pumped for transportation, avoiding significant compression costs as for classical CO_2 capture units (where carbon dioxide is discharged in gas phase and at atmospheric pressure), and further uses such as Enhanced Oil Recovery (EOR) or underground storage.

In this paper, the three most common natural gas low-temperature purification techniques have been modelled and their performances have been evaluated through energy and exergy analyses. Specifically, the dual pressure low-temperature distillation process, the anti-sublimation process and a hybrid configuration have been considered. It is found that the dual pressure low-temperature distillation scheme reach the highest thermodynamic performances, resulting in the best values of exergy efficiency and equivalent methane requirements with respect to the other configurations. This is mainly due to the distributed temperature profile along a distillation column, resulting in a less irreversible heat exchanging process.

Keywords: LNG, exergy analysis, natural gas purification, carbon dioxide

Highlights:

- Low-temperature processes for of high CO_2 content natural gas have been modelled;
- Energy and exergy analyses have been performed;

- The Dual Pressure distillation scheme has the best thermodynamic performances;
- There is a synergy between cryogenic natural gas purification and LNG production;

1. Introduction

1.1. The synergic potential of low-temperature natural gas purification processes and LNG production

According to the known geographic distribution of gas reserves, almost 40% of the global reserves are sour [1] and about 30% have a CO_2 contents between 15% and 80% [2,3]. Sour and acid gas reserves are located in different geographic areas, such as South-East Asia, North Africa, Middle East, USA and Australia [2]. As instances, the giant *Natuna* field in Indonesia is characterized by a CO_2 content higher than 70%; the *Kapuni* field in New Zeland with a CO_2 content of about 43.8% [4]; the *Uch* field in Pakistan with 46.2% of CO_2 [4]; the *LaBarge* field in Wyoming (USA) of about 65% [5].

In last decades, low-temperature processes for the purification of highly acid and/or sour gas reserves have started to gain attention. Beside classical and worldwide adopted absorption processes, above all chemical scrubbing by means of aqueous alkanolamine solutions, low-temperature processes allow to reduce the total operating costs when dealing with gases containing high amounts of CO_2 [6,7]. According to authoritative projections of future energy scenarios [8], the primary energy demand is expected to grow rapidly over the next twenty years: natural gas will play a key role, resulting in the highest growth trend [9]. For such reason, it is relevant to investigate alternative purification processes, able to perform a profitable exploitation of acid and sour natural gas reserves.

Several types of low-temperature natural gas purification technologies can be found in literature. Since these processes operate at temperatures below the triple point of CO_2, one of their major concerns resides in the formation of a CO_2 solid phase inside the system. These processes can be classified into two main groups according to how the CO_2 is treated: processes designed to handle the formation of a solid phase inside equipment and processes that avoid the CO_2 freeze-out. The first group includes the *CFZ*™ process by Exxon Mobil [5,10–14], the *Cryocell*® process [15,16], the *Cryopur*® process [17] based on the anti-sublimation technique [18] and the integrated cryogenic CO_2 removal coupled with pressurized natural gas liquefaction [19]. The second group of low-temperature natural gas purification processes includes: the *Ryan-Holmes* process [20–22] where an entrainer (normally a hydrocarbon heavier than methane, such as n-butane) is used to shift CO_2 freezing conditions at lower temperatures and pressures; the *Sprex*® process [23,24] where a bulk CO_2 removal is performed in a pressurized low-temperature distillation column, operated away from freezing conditions, while the final purification of the gas is made with a traditional MDEA unit and, recently, a new patented low-temperature dual pressure distillation process [7,25] designed to bypass the freezing point of CO_2 in mixtures with methane by means of a specific thermodynamic cycle. The final product of low-temperature purification processes consists in a high-purity methane stream at low-temperatures and at pressures depending on the selected technology (typically distillation is performed under pressure, while anti-sublimation is performed at pressures below the triple point one of CO_2), while CO_2

is recovered as a pressurized liquid phase, which is suitable to be pumped and transported for further purposes: *Enhanced Oil Recovery* (EOR) or *Carbon Capture and Storage* (CCS).

From a technical perspective, transport of natural gas in liquid phase [26] (1.01325 bar and 113.15 K) is favored when distances are higher than 3500 km [27]. Other aspects, such as geopolitics and safety issues [27], should be taken into account when selecting natural gas transport as LNG. Mostly, the mismatch between the geographic location of gas production sites and end-markets [28–30] is a key-driver for the development of the LNG market [27,30]. Recent studies show that LNG trades are continuously growing [31], even if forecasting the future market is difficult due to the variations in energy prices, the volatility of regional markets, the competition with other sources of natural gas and the ever-changing economic situations of different countries [32]. Despite this, the growing importance of LNG in the global energy market [33–37] can be highlighted considering the increase in liquefaction train sizes from 1960 to 2011, from less than 1 MT y^{-1} (Algeria) up to 8 MT y^{-1} (Quatargas and RasGas) [32]. The global LNG trade is expected to grow in a significant way, giving the major contribution to the expansion, integration and flexibility of the global natural gas market [9].

Several natural gas liquefaction technologies have been proposed for the production of LNG [38]. Mostly these processes perform the liquefaction by means of Mixed Refrigerant Cycles (MRC) [39], cascade cycles with pure component refrigerants and expansion processes where a turboexpander is used instead of a Joule-Thomson (JT) valve [27,40]. The works by Lim et al. and Chang [27,40] offer a detailed overview of industrial processes for the liquefaction of natural gas. These processes are applied mainly to the large-scale LNG production, with the inlet gas feed under pressure and at temperatures close to the ambient one. Low-temperature natural gas purification processes provide liquefied natural gas at high pressure and low-temperatures (about 173.15 K) [41]. In such processes, part of the overall cooling duty required for the production of LNG is supplied during the purification step.

1.2. Aim of the work

This work contributes in the synergistic coupling of low-temperature natural gas purification processes and LNG production processes. Specifically, this work assesses the thermodynamic performances of different low-temperature natural gas purification processes with LNG production through energy and exergy analysis. Different technically feasible low-temperature process layouts are here considered:

1. The *dual pressure distillation proc*ess proposed by Pellegrini [25]. This process allows the removal of carbon dioxide without incurring in freezing conditions in a distillation unit. Moreover, this process does not require any *ad-hoc* designed equipment and/or third components to prevent CO_2 freeze-out (i.e. relevant regeneration and recycle facilities);
2. The *anti-sublimation process* [17]. This process allows to remove dry ice directly over the surface of a dedicated heat exchanger, giving compactness to the process solution;
3. The *hybrid process* is the combination of a pressurized distillation column, that performs only a bulk purification so avoiding solid CO_2 formation, with heat exchangers for anti-sublimation for the finishing action; such configuration should present intermediate performances when compared with the previous ones.

Basing on the authors knowledge, in the open literature no other works about the detailed study and assessment (on both energy and exergy bases) of the coupling of innovative low-temperature natural gas purification processes with cryogenic LNG production are present. This work aims to better investigate the possibilities of an effective combination of these low-temperature technologies with LNG production, considering also a possible combination of two low-temperature natural gas purification processes in order to determine which solution allows to obtain the best performances, minimizing the consumptions of external fuels and, at the same time, optimizing the use of energy. Moreover, this paper aims to show that the combination of energy and exergy analysis can provide a reliable tool to better screen process technologies and their interaction, defining moreover possible pathways for process optimization.

2. Thermodynamic framework

In order to better investigate the thermodynamic behavior of the considered processes, phase equilibria calculations have been performed by means of Aspen Hysys® V7.3 [42], relying on the SRK Equation of State (EoS) [43] and predicting the solid CO_2 formation by means of the CO_2 Freeze-out utility. The reliability of the selected simulation framework has been already validated through a comparison with literature available experimental data [7,44].

The phase behavior of the binary system $CH_4 - CO_2$ at different pressure is essential for this study: it is well known in literature and it has been studied by several authors [44–49]. Specifically, the Pressure-Temperature (PT) diagram of the mixture (Figure 1) is of Type-I according to the Van Konynenburg and Scott [50] classification of phase diagrams.

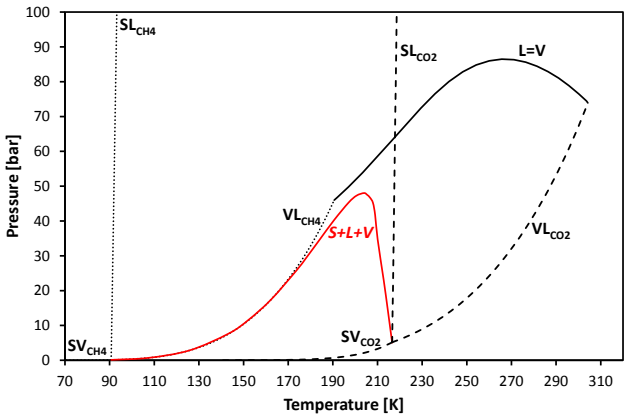

Figure 1. PT diagram of the CH4-CO2 system [7].

It is possible to notice that the Solid-Liquid-Vapor Equilibrium (SLVE) locus presents a pressure maximum and his left part, which goes from the maximum to the triple point of pure CH_4, is close to the Vapor-Liquid Equilibrium (VLE) line of pure CH_4. In this way, at low-temperatures, the temperature difference between SLVE and VLE of pure methane is narrow. The maximum pressure of the SLVE locus is above the critical one of pure CH_4, hence, it is not possible to obtain pure methane avoiding CO_2 freeze out by means of a

single distillation unit at constant pressure. As can be inferred from the graph, CO_2 freezing at triple point occurs at any pressure below about 50 bar.

The low-temperature distillation process considered in this work has been designed to operate

at two different pressures (50 bar and 40 bar) in order to bypass the SLVE locus of the mixture [7,25]. The phase equilibria in these conditions can be better visualized by means of isobaric diagrams (Figure 2).

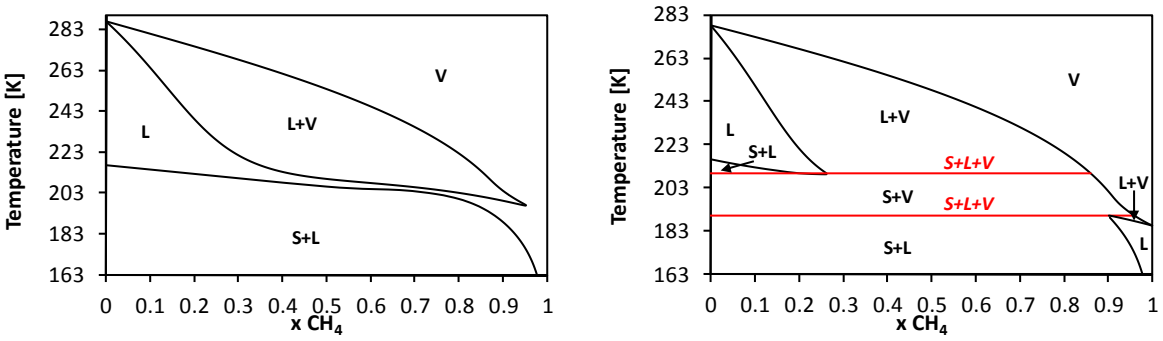

Figure 2. Isobaric diagrams at 50 bar (left side) and 40 bar (right side) for the $CH_4 - CO_2$ system [7].

When pressure is decreased from 50 bar to 40 bar the SLVE locus is crossed twice and the VLE region is separated by a Solid-Vapor Equilibrium (SVE) region at temperatures between the two SLVE ones. The behavior of the system is similar when pressure is furthermore decreased: the SVE region enlarges and the VLE region at higher temperatures reduces till the triple point pressure of pure CO_2. Below this pressure, VLE equilibrium for pure CO_2 does not exist anymore and the SLVE locus is crossed only at one temperature close to the VLE one of pure CH_4.

These conditions are suitable to operate the anti-sublimation process [17], that is the second process considered in this work, by frosting CO_2 at SVE leaving few ppms in the main methane stream, avoiding at the same time the formation of a liquid phase in the system. In order to reach high methane purities avoiding extremely low temperature levels, it is not possible to operate the purification in the SLE region at low pressures. This concept is better explained considering the isobaric diagram at 1 bar (Figure 3).

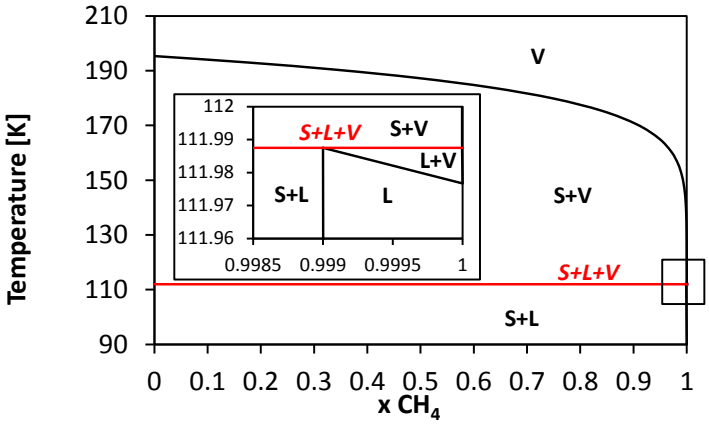

Figure 3. Isobaric diagram at 1 bar for the $CH_4 - CO_2$ system.

From the Figure 3 it is possible to notice that the system presents a wide SVE region at temperatures down to the SLVE one. Below this temperature, a Solid-Liquid Equilibrium (SLE) and a narrow VLE region exist. The VLE region is present at very high methane concentrations and in a small temperature range. In this way, it is possible to obtain anyway methane in liquid phase also at low pressures (for instance higher than the triple point pressure of pure methane).

Thus, when a distillation technology is adopted for LNG production, the purity of the produced methane should be high enough to avoid the formation of a CO_2-rich solid phase during expansion from high pressures to the atmospheric one at which LNG is stored. During the anti-sublimation process, the formation of a solid phase during expansion may occur and solid CO_2 is separated from methane in SVE conditions at low pressures.

3. Description of the process schemes' layout

Three different process schemes for the production of LNG have been considered in this work. The material streams at battery limits are the same for each considered configuration. The low-temperature purification technology adopted in each process is different: as introduced in sub-section 1.2, a dual pressure distillation, an anti-sublimation on heat exchangers surfaces and a coupling of the previous ones is here considered.

3.1. Process schemes design specifications

The natural gas stream, considered as a binary $CH_4 - CO_2$ mixture with 40 mole % of CO_2, is separated in order to recover liquefied CO_2 and pure CH_4. The material balances across the battery limits are summarized in Table 1.

A flow rate of 5000 kmol h^{-1} of natural gas with high CO_2 content, available at 50 bar and at 308.15 K, is the feed to all the process schemes. The pressure is consistent with that of natural gas at the wellhead and such to prevent CO_2 freeze-out in distillation process equipment. The final product in all the considered case-studies is LNG at 1.01325 bar: the target purity for the liquefied gas has been fixed at 50 ppm of CO_2, as recommended for LNG production [51] to avoid freezing problems during liquefaction. To achieve the liquefaction of the produced stream (methane at the required high-purity) is necessary to provide cooling duties at a temperature of about 111.75 K. The by-product of the processes is a stream of liquid CO_2 available at 50 bar and a mole fraction of CH_4 limited to 100 ppm in order to enhance the CH_4 recovery [25]. . These conditions are suitable for its transport and further uses, such as: reinjection for permanent storage (CCS) or Enhanced Oil Recovery (EOR) [5,16,25,52].

Table 1. Molar streams specifications at battery limits.

Stream	x_{CH4}	x_{CO2}	F [kmol h^{-1}]	T [K]	P [bar]
INLET NG	0.6	0.4	5000	308.15	50
LNG	0.99995	5e-5	~3000	111.75	1.01325
Liquid-CO2	1e-4	0.9999	~2000	287.21	50

3.2. Process scheme layouts

The layouts of the three simulated processes are here presented: the dual-pressure distillation process (1), the anti-sublimation process (2) and hybrid process (3). The main features of the considered processes and their relative simulation approaches are summarized in Table 1.

Process simulations have been performed through *Aspen Hysys*® V7.3, considering the SRK EoS [43] as the thermodynamic package for calculations. However, this software is not able to perform detailed process simulations considering the presence of a solid phase: for this reason, it has been applied only to simulate process equipment that handle fluid phases. In order to estimate energy consumptions and to verify the heat recovery feasibility for equipment in which dry ice formation occurs, material and enthalpy balances have been evaluated separately.

Table 2. Process scheme layout features.

Scheme number	Purification step approach	Purification step temperature	Simulation tools
1	Distillation	Low temperature	Aspen Hysys®
2	Anti-sublimation	Cryogenic	Aspen Hysys® plus thermodynamic balances
3	Distillation and anti-sublimation in series	Low temperature and cryogenic in series	Aspen Hysys® plus thermodynamic balances

Correlations for the evaluation of heat capacities for CO_2 and CH_4 in gaseous and liquid phases have been derived from literature [53–55]. The evaluation of heat capacity of solid CO_2 (in J mol^{-1} K^{-1}) has been performed using the polynomial Equation (1), where the constant coefficients have been evaluated regressing the experimental data reported by Giauque and Egan [56]: the correlation well fits experimental data (Fig. 4). The phase change enthalpies used to solve the energy balances have been collected in Table 3.

$$c_{p,CO2}^{S} = -33.972 + 1.820T + -1.810 \cdot 10^{-2} T^{2} + 8.600 \cdot 10^{-5} T^{3} - 1.496 \cdot 10^{-7} T^{4} + 188.173 \cdot T^{-1} \quad (1)$$

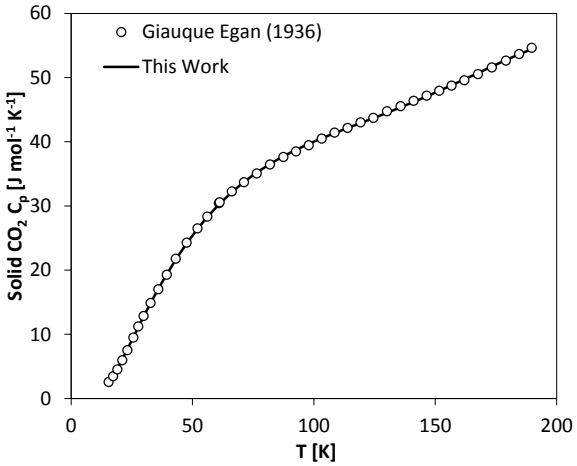

Figure 4. Comparison between experimental data [56] and equation (1) for solid CO_2 heat capacity.

In the following sections, the process scheme layouts are presented by means of block flow diagrams (BFDs). Red boxes have been used in Figure 6 and Figure 10 to highlight the unit operations simulated with Aspen Hysys® V7.3. The properties of the main inlet and outlet streams are reported in Table 1 and are the same for all the three presented processes.

Table 3. CO_2 and CH_4 thermo-physical properties for balance calculation: phase change enthalpies.

Parameter	Value [kJ mol^{-1}]	Reference
Δh_{CO2}^{sub} (183.15 K)	26.20	[57]
Δh_{CO2}^{ev} (215.65 K)	15.33	[58]
Δh_{CO2}^{fus} (T_{triple})	8.65	[59]
Δh_{CH4}^{ev} (111.65 K)	8.15808	[59]

3.2.1. Dual Pressure Low-Temperature Distillation process

In the scheme of Figure 5, the natural gas purification is performed by means of the dual pressure low-temperature distillation process [25]. In this process, the purification section consists of two distillation columns: the first one is operated at high pressure (HP, 50 bar), above the maximum of the SLVE curve of the PT diagram (Figure 1), while the second one at low pressure (LP, 40 bar), below the methane critical pressure. The number of theoretical stages for distillation columns has been chosen considering a qualitative trade-off between energy consumptions and investment costs (referring to natural gas purification technologies by means of distillation [21, 24]) and considering the LNG purity specifications, that are much more stringent than pipeline-quality gas ones. In particular, for process scheme 1, 25 and 20 theoretical trays have been adopted for the distillation columns employed, respectively, while in the original patent [25] 20 and 15 theoretical trays have been used to produce pipeline-quality gas (i.e. about 2 mol% of CO_2). With this configuration, the duties required at reboiler and condenser of the dual pressure low-temperature distillation process are similar to the ones of the original patent [25]**.** The HP column can be regarded as the stripping

section of a common distillation column: it presents only a reboiler, while the liquid reflux is provided by recycling the liquid stream coming from the bottom of the LP section. In the same way, the LP column works as the enrichment section of a classic distillation column: it has a partial condenser on the top and the gas feed stream is the top product from the HP section. The product gas stream from the top of LP column is composed mainly of methane at the required purity specifications. LNG is then produced by means of a proper liquefaction train. It has been assumed that this section consists of a gas turbine followed by a cooler. The bottom product from the purification section is highly pure CO_2 (Table 1).

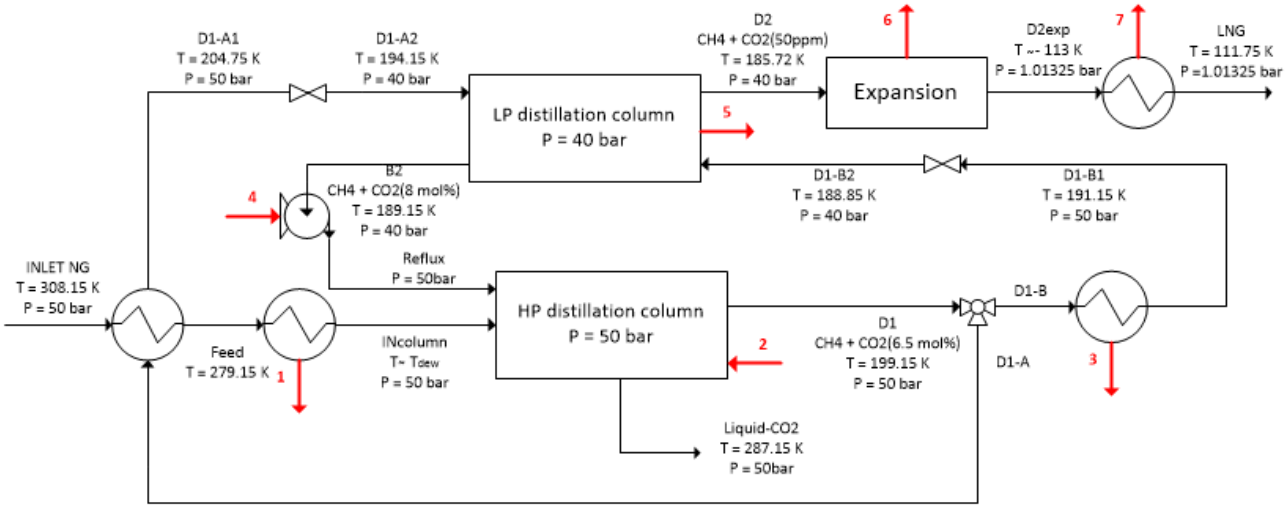

Figure 5. Layout of the dual pressure low-temperature distillation process.

The *INLET NG* stream is fed at the conditions reported in Table 1. Before entering the HP distillation column, it is cooled down to its dew point at 50 bar (*INcolumn*) using two heat exchangers in series. In the first heat exchanger, the *INLET NG* stream is precooled using stream *D1-A*, that needs to be heated (*D1-A1*) to provide a superheated gas stream (*D1-A2*) after expansion to the pressure of the LP section, in order to avoid CO_2 freezing at the inlet of the LP column. The precooled Feed stream is furthermore cooled down to reach its dew point in a second heat exchanger, using an external utility, before entering the HP section of the distillation unit (*INcolumn*). According to the phase behavior of the $CO_2 - CH_4$ mixture (see Figure 1 to Figure 3), no freezing can occur during distillation at about 50 bar. The HP section performs a bulk removal of the inlet CO_2: the bottom stream is liquid CO_2 at high pressure, while the top product stream is the methane-rich stream *D1* (with about 6.5 mole % of CO_2). Since the HP section operates at a pressure above the methane critical one (45.9 bar [54]), it is not possible to obtain pure methane performing distillation at 50 bar. The final purification is performed in the LP section, operated at about 40 bar. The produced streams from the LP section are a top methane gas stream and a bottom methane-rich liquid stream that is pumped back to the HP section. The *INcolumn* stream enters the HP column on the fourth tray from the top, while the liquid reflux (*Reflux*) is introduced at the first tray from the top. The over gas stream *D1* from the HP section is sent to a splitter, which separates it into two streams (*D1-A* and *D1-B* respectively). Before entering the bottom of the LP section, stream *D1-A* is heated up (*D1-A1*) and expanded to the LP section pressure (*D1-A2*) 5-6 K over its dew point at the pressure of the LP section. This guarantees that no solid phase can be

formed during its expansion. Stream *D1-B* is cooled down (*D1-B1*) at 50 bar (away from the SLE boundary) and expanded to the LP section pressure in order to obtain a liquid stream at its bubble point (*D1-B2*), that is fed in turn to the LP section one theoretical tray above the gas feed stream *D1-A2*. The *D1*A/D1B split factor is chosen in order to keep the CO_2 level in the *Reflux* stream below 8 mole % to avoid CO_2 freezing. The reflux ratio for the LP distillation has been set to 2.4.

3.2.2. Anti-sublimation process

The LNG production by means of the anti-sublimation process (Figure 6) adopts the anti-sublimation technique on heat exchanger surfaces to perform natural gas purification. In this process, the purification is performed allowing dry ice formation in a closed and dedicated unit operation. Several studies on this technology can be found in literature, where this process is often applied to CO_2 removal from flue gases and biogas, investigating the dry ice formation on heat exchanger surfaces and to perform thermodynamic and energy evaluations [60–66]. In the scheme presented in Figure 6, two heat exchangers are operated in dynamic mode, realizing the *operation* (*Anti-sublimation Heat Exchanger* AHE) and *regeneration* (*Recovery Heat Exchanger* RHE) phases, and ensuring the continuous operation of the process. Different line styles (solid or dashed) have been adopted in order to describe the material flows direction according to the working phase alternation: solid lines are used for the operation phase, while dashed for the regeneration one.

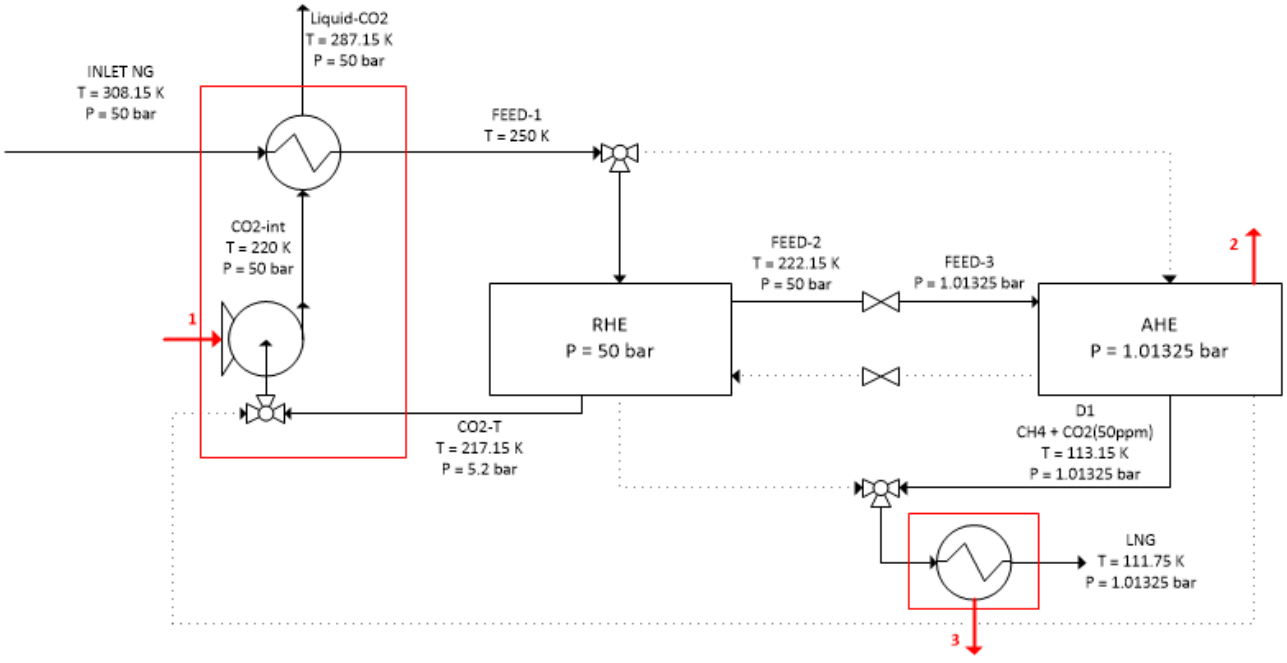

Figure 6. Layout of the anti-sublimation process.

The *INLET NG* stream is fed to the process at the conditions in Table 1. The stream is sent to a heat exchanger where it is cooled down to stream *FEED-1*. The amount of heat recovery is defined in order to warm the liquid stream CO_2-int up to 287.21 K at 50 bar, assuming a minimum temperature approach of

about 5 K. The stream *FEED-1* is fed to RHE. The dry ice layer deposited during the previous operating cycle, when the c RHE worked as AHE, provides part of the cooling duty to *FEED-1*. *FEED-1* is cooled down to 222.15 K (*FEED-2*) by melting the dry ice that is recovered as liquid CO_2 at its triple point (*CO_2-T*). In order to avoid pinch cross problems a minimum approach equal to 5 K ($\Delta T_{min,RHE}$) is kept between the temperatures of stream *FEED-2* and of stream *CO_2-T*. The *CO_2-T* stream is then pumped to 50 bar (*CO_2-int*) and heated in a heat recovery equipment where coupling of the *CO_2-int* stream with *INLET NG* one takes place. The stream *FEED-2* from RHE, at VLE, is expanded from 50 bar to the atmospheric pressure by means of a Joule-Thomson (JT) valve and turns into *FEED-3*. To achieve CO_2 anti-sublimation (Figure 3) it is necessary to expand the stream to a pressure level below the CO_2 triple point pressure (5.2 bar [64]).The stream *FEED-3* enters the AHE, where it is cooled down. The cooling duty necessary to perform the CO_2 anti-sublimation is supplied by an external refrigeration cycle. During the expansion process, an amount of dry ice separates from the main stream in SVE. To reach the purity specification required for LNG production, a further CO_2 separation is necessary and it is accomplished cooling the gas stream down to 113.15 K ($T_{CO2,frosting}$). Inside the AHE, a solid CO_2 layer grows and a gas stream with 50 ppm of CO_2 (*D1*) is available at atmospheric pressure and can be liquefied for LNG production. A heat exchanger using an external cooling medium is used for the purpose. Once the RHE is cleaned and ready to support dry ice formation and the AHE presents a solid CO_2 layer that needs to be liquefied and recovered, a switch between RHE and AHE is performed to assure continuity in natural gas stream purification and liquefaction. Since CO_2 solid phase formation occurs, the anti-sublimation process has been simulated according to heat and material balances across RHE and AHE.

With reference to Figure 7, RHE has been assumed to operate globally in adiabatic mode. To allow the feasibility of the heat recovery process, the heat $\dot{Q}_{CO2}^{IN}$, calculated using relation (2), must not be less than $\dot{Q}^{OUT}$, calculated through the energy balance expressed by relations (3) to (5). In the case that $\dot{Q}_{CO2}^{IN}$ is higher than $\dot{Q}^{OUT}$, further solutions can be adopted to liquefy the remaining dry ice. The thermodynamic cycle shown in Figure 8 is useful to understand CO_2 phase changes: the solid lines represent the path followed in order to calculate $\dot{Q}_{CO2}^{IN}$ using Equation (2).

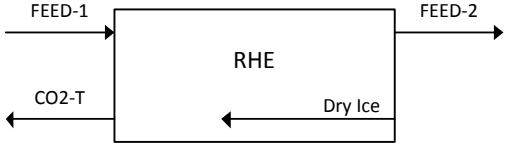

Figure 7. RHE scheme for energy balance in the anti-sublimation process.

$$\dot{Q}_{CO2}^{IN} = \dot{n}_{CO2-T} \cdot \left[\Delta h_{CO2}^{sub}(T_{CO2,\,frosting}) + \int_{T_{CO2,\,frosting}}^{(T_{FEED-2} - \Delta T_{\min,\mathrm{RHE}})} Cp_{CO2}^{G}(T)\,dT + \Delta h_{CO2}^{cond}(T_{FEED-2} - \Delta T_{\min,\mathrm{RHE}}) \right] \quad (2)$$

$$\dot{H}_{FEED-1}(T) = \dot{n}_{CH4} \cdot \left[\tilde{h}_{rif}(T_{rif}) + \int_{T_{rif}}^{T_{IN}} Cp_{CH4}^{G}(T)\,dT \right] + \dot{n}_{CO2} \cdot \left[\tilde{h}_{rif}(T_{rif}) + \int_{T_{rif}}^{T_{IN}} Cp_{CO2}^{G}(T)\,dT \right] \quad (3)$$

$$\dot{H}_{FEED-2}(T) = \dot{n}_{FEED-2} \cdot \frac{V}{F} \left\{ y_{CH4} \cdot \left[\tilde{h}_{rif}(T_{rif}) + \int_{T_{rif}}^{T_{OUT}} Cp^{G}_{CH4}(T)\,dT \right] + y_{CO2} \cdot \left[\tilde{h}_{rif}(T_{rif}) + \int_{T_{rif}}^{T_{OUT}} Cp^{G}_{CO2}(T)\,dT \right] \right\} +$$
$$+ \dot{n}_{FEED-2} \cdot (1 - \frac{V}{F}) \cdot \left\{ x_{CH4} \cdot \left[\tilde{h}_{rif}(T_{rif}) + \int_{T_{rif}}^{T_{OUT}} Cp^{G}_{CH4}(T)\,dT - \Delta h^{ev}_{CH4}(T_{OUT}) \right] \right\} + \quad (4)$$
$$+ \dot{n}_{FEED-2} \cdot (1 - \frac{V}{F}) \cdot \left\{ x_{CO2} \cdot \left[\tilde{h}_{rif}(T_{rif}) + \int_{T_{rif}}^{T_{OUT}} Cp^{G}_{CO2}(T)\,dT - \Delta h^{ev}_{CO2}(T_{OUT}) \right] \right\}$$

$$\dot{Q}^{OUT} = \dot{H}_{FEED-1}(T_{IN}) - \dot{H}_{FEED-2}(T_{OUT}) \quad (5)$$

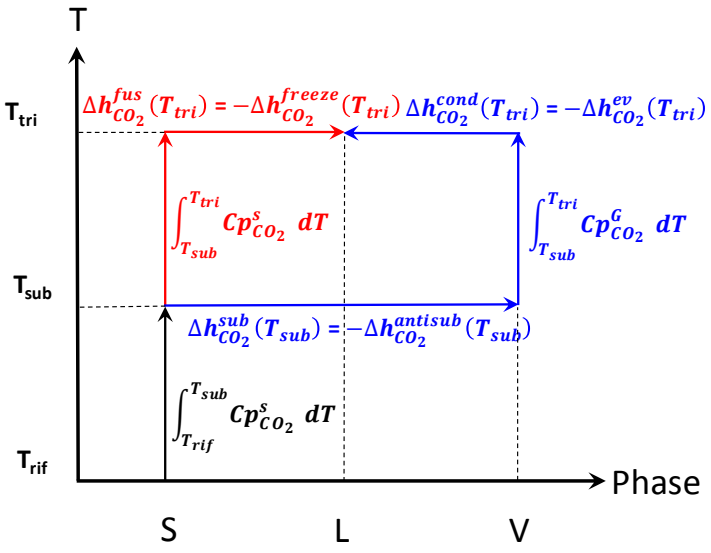

Figure 8. Thermodynamic cycle for CO_2 phase changes.

The duty removed by an external cooling medium through a refrigeration cycle is $\dot{Q}^{OUT}$, and it is calculated according to Equation (6). The AHE control volume (Figure 9) includes also the JT valve. The different terms in balance (6) can be evaluated using Equations (4), (7) and (8).

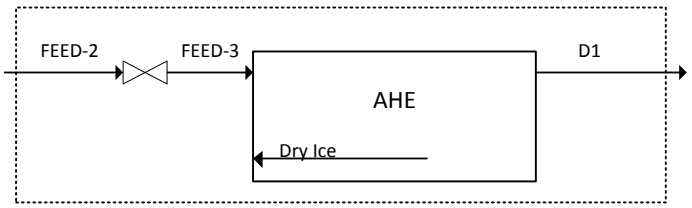

Figure 9. AHE scheme for energy balance in the anti-sublimation process.

$$\dot{H}_{FEED-2}(T) = \dot{H}_{D1}(T) + \dot{H}_{DryIce}(T) + \dot{Q}_{OUT} \quad (6)$$

$$\dot{H}_{D1}(T) = \dot{n}_{D1} \cdot \left\{ y_{CH4} \cdot \left[\tilde{h}_{rif}(T_{rif}) + \int_{T_{rif}}^{T_{OUT}} Cp^{G}_{CH4}(T)\,dT \right] + y_{CO2} \cdot \left[\tilde{h}_{rif}(T_{rif}) + \int_{T_{rif}}^{T_{OUT}} Cp^{G}_{CO2}(T)\,dT \right] \right\} \quad (7)$$

$$\dot{H}_{DryIce}(T) = \dot{n}_{DryIce} \cdot \left[\tilde{h}_{rif}(T_{rif}) + \int_{T_{rif}}^{T_{OUT}} Cp^{G}_{CO2}(T)\,dT - \Delta h^{sub}_{CO2}(T_{OUT}) \right] \quad (8)$$

3.2.3. Hybrid process

The hybrid process presented in Figure 10 combines the purification approaches of processes 1 and 2. For this process, the distillation column used to realize the first part of the purification process has 25 ideal trays as the HP pressure section of the process considered in process 1.

The natural gas stream rich in CO_2 is fed to a distillation column operated at 50 bar, whose design is similar to the one of the HP section of process 1. The difference is the presence of a condenser at the top of the distillation column, which is necessary to ensure the liquid recirculation. The distillation column performs a bulk removal of CO_2. The produced top gas stream has a CO_2 content close to 10 mole %. The heat exchangers in series allow to clean the gas stream in order to reach the specifications required for liquefaction. As well as for process 2, two identical devices (RHE and AHE) are operated in parallel in an alternate mode, in order to allow continuous operation. For the sake of clearness, only one operation phase is reported in Figure 10, where solid line represents the flow of natural gas throughout the process. With reference to Figure 10, RHE heat exchanger is assumed to operate in recovery phase, while the AHE works in anti-sublimation phase.

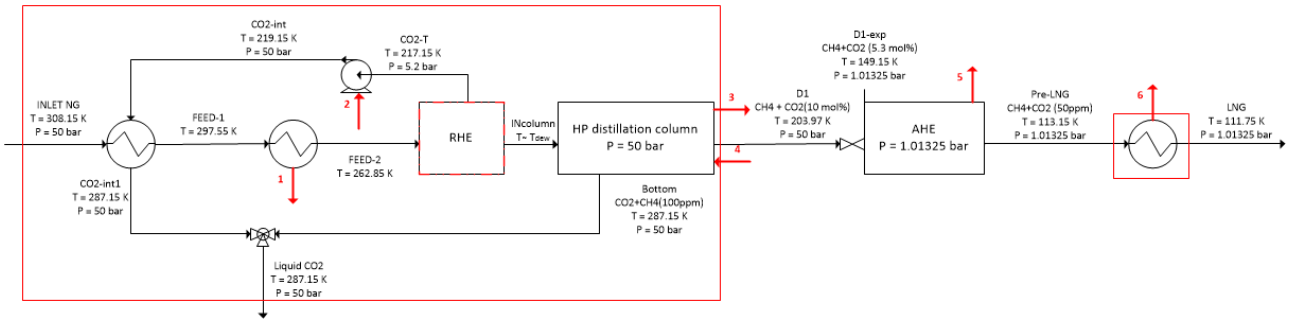

Figure 10. Hybrid process layout.

The *INLET NG* stream specifications are summarized in Table 1. Before being fed to the HP distillation column, *INLET NG* is cooled at its dew point at 50 bar (*INcolumn*) by means of three heat exchangers in series. In the first heat exchanger, the *INLET NG* stream is cooled by heat recovery with the process stream CO_2*-int*. The heat recovery is defined in order to warm CO_2*-int* up to 287.21 K at 50 bar, assuming a minimum approach temperature of 5 K. The CO_2*-int* stream becomes then CO_2*-int2* and it can be mixed with the *Bottom* stream (the CO_2-rich liquid stream extracted from the bottom of the HP distillation column) to give the stream *Liquid-*CO_2. The cooled *INLET NG* stream becomes *FEED-1* that is sent to a heat exchanger where an external utility is used to cool this stream down to *FEED-2*. A second heat recovery occurs inside the

RHE, where the solid CO_2, formed during the previous operating cycle, is melted to produce a liquid CO_2 stream at its triple point (*CO_2T*). The necessary heat amount, after exclusion of pinch problems, can be provided by *FEED-2* that needs to be cooled down in order to reach the *INcolumn* stream conditions, i.e. dew point at 50 bar. The liquefied CO_2 stream is recovered at its triple point (*CO_2-T*) and is pumped (*CO_2-int*) and heated (*CO_2-int2*) in order to be mixed with the stream *Bottom*. The distillation column is operated at 50 bar and it has 25 theoretical trays. The feed stream *INcolumn* enters on the third tray from the top. The bottom product (*Bottom*) is a pressurized liquid CO_2-rich stream under pressure, while, from the top, a gas product stream (*D1*) rich in methane is obtained. The content of CO_2 in *D1* is 10 mole % due to the limitation of the critical conditions. The stream *D1* is then expanded to the atmospheric pressure by means of a JT valve and furthermore cooled down 113.15 in AHE. This process allows to accomplish a CO_2 separation from the main gas stream in order to meet the purity specifications for LNG production. Inside the AHE a dry ice layer is formed and, in the subsequent operating cycle, it will be recovered as liquid CO_2 at its triple point. The methane-rich gas stream (*Pre-LNG*) produced from the AHE is then liquefied in a heat exchanger by means of an external cooling medium in order to obtain LNG ready for commercialization.

In order to verify the feasibility of the proposed heat recoveries, the energy balances must be verified for both the heat exchangers.

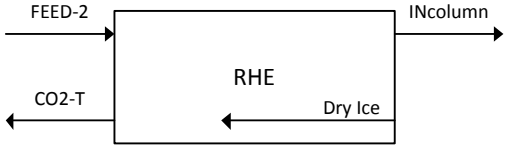

Figure 11. RHE scheme for energy balance in the hybrid process.

As for the anti-sublimation process, and with reference to Figure 11, RHE has been assumed to operate adiabatically. In this way, the energy balance is used to verify the feasibility of the internal heat recovery, and the required duty useful to liquefy the dry ice layer is calculated according to Equation (9).

$$\dot{Q}_{CO2}^{IN} = \dot{n}_{CO2-T} \cdot \left[\Delta h_{CO2}^{sub}(T_{CO2,\,frosting}) + \int_{T_{CO2,\,frosting}}^{(T_{FEED-2} - \Delta T_{\min,\mathrm{RHE}})} Cp_{CO2}^{G}(T)\,dT + \Delta h_{CO2}^{cond}(T_{FEED-2} - \Delta T_{\min,\mathrm{RHE}}) \right] \quad (9)$$

In AHE (Figure 12), the duty $\dot{Q}^{OUT}$, removed by the external cooling medium through a refrigeration cycle, is calculated according to the balance presented in Equation (10).

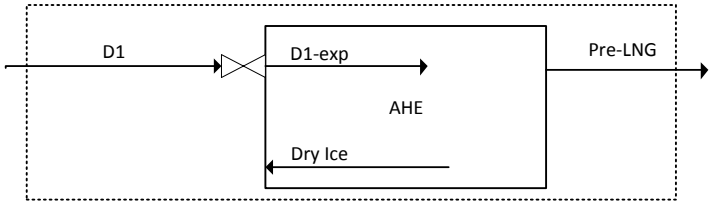

Figure 12. AHE scheme for energy balance.

$$\dot{H}_{D1}(T) = \dot{H}_{pre-LNG}(T) + \dot{H}_{DryIce}(T) + \dot{Q}_{OUT} \tag{10}$$

The different terms in Equation (10) can be evaluated using Equations (11), (12) and (13).

$$\dot{H}_{pre-LNG}(T) = \dot{n}_{pre-LNG} \cdot \left\{ y_{CH4} \cdot \left[\tilde{h}_{rif}(T_{rif}) + \int_{T_{rif}}^{T_{OUT}} Cp_{CH4}^{G}(T)\,dT \right] + y_{CO2} \cdot \left[\tilde{h}_{rif}(T_{rif}) + \int_{T_{rif}}^{T_{OUT}} Cp_{CO2}^{G}(T)\,dT \right] \right\} \tag{11}$$

$$\dot{H}_{DryIce}(T) = \dot{n}_{DryIce} \cdot \left[\tilde{h}_{rif}(T_{rif}) + \int_{T_{rif}}^{T_{OUT}} Cp_{CO2}^{G}(T)\,dT - \Delta h_{CO2}^{sub}(T_{OUT}) \right] \tag{12}$$

$$\dot{H}_{D1}(T) = \dot{n}_{D1} \cdot \left\{ y_{CH4} \cdot \left[\tilde{h}_{rif}(T_{rif}) + \int_{T_{rif}}^{T_{OUT}} Cp_{CH4}^{G}(T)\,dT \right] + y_{CO2} \cdot \left[\tilde{h}_{rif}(T_{rif}) + \int_{T_{rif}}^{T_{OUT}} Cp_{CO2}^{G}(T)\,dT \right] \right\} \tag{13}$$

4. Analysis of the low-temperature purification processes

In this section, thermodynamic performances of the low-temperature purification processes introduced in section 3 are assessed by means of energy and exergy analyses. Energy analysis is performed according to the *Net equivalent methane method* [67]: it accounts for the amount of methane required by defined reference processes to deliver thermal and mechanical energy to each one of the analyzed process. On the other hand, exergy analysis is performed according to the traditional exergy method, formalized among others by Kotas [68] and Bejan [69]. Results are finally presented and discussed.

Both the approaches are able to harmonize the different nature of the energy interactions involved in each process: indeed, thermal, mechanical and bulk flows that cross system boundaries are characterized by means of their energy or exergy equivalents, ensuring a coherent assessment of the thermodynamic efficiency for each process.

4.1. Net equivalent methane and Exergy analyses

The *Net equivalent methane analysis* can be performed by converting all the energy interactions between the analyzed process and the external environment into an equivalent amount of methane that is required to provide such interactions by means of conventional engineering processes. Therefore, assumptions are

made on the technology used to produce the required energy flows absorbed by the system: steam generation, electricity for compressors or pumps and vapor-compression refrigeration cycles. On the other hand, all the energy that is produced by the system as a by-product is considered as a saving of methane (providing that it is easily recoverable): as an instance, the electricity obtained from expanding flows by means of turbines, or hot mass flows (temperature above 373.15 K) that need to be cooled down can be seen as useful by-products.

On the other hand, *Exergy analysis* allows take into account both quantity and quality of energy streams flowing through the layout boundaries, uniformly expressing them by means of their mechanical energy equivalents, thus allowing to remove the hypotheses required by the Net equivalent methane method [68,70–72]. This feature is particularly relevant in modern economies, where energy utilities are produced by different kind of technologies, and where distributed generation and penetration of renewables are continuously increasing [73–75].

The definition of reference environmental conditions is an implicit prerequisite for the evaluation of exergy, which is a property of both the system and the environment: the *Baher* reference environment is here assumed and distinguished by the subscript "0", with a temperature of 298.15 K and a pressure of 1.01325 bar [76].

With reference to Table 4, the conventions required to evaluate the equivalent methane and the exergy of energy and bulk flow interactions that characterize the analyzed system are following listed.

Work interactions. The electric and mechanical energy flows that cross the boundary of the analyzed process are accounted by the net equivalent methane method as the methane consumed or saved by a classic combined cycle power plant with energy efficiency η_{CC} of 0.55 [77]. Such efficiency is defined as the ratio between the net power output $\dot{W}_{el}$ and the thermal power input $\dot{Q}_{CH4}^{W}$ coming from the combustion of methane (with an heating value LHV_{CH4} of 50 MJ kg^{-1} [54]). Differently, Exergy analysis accounts for the exergy equivalent of the stream, which is numerically equal to the work interaction. The direction of the equivalent methane and the exergy flows are the same of the considered work interaction [78].

Heat interactions. If the thermal energy is removed by the analyzed process, it is accounted by the Net equivalent methane method as the energy required to drive a classic vapor-compression refrigeration cycle with a Second Law efficiency $\eta_{II,f}$ equal to 0.6 [27,79,80]. The mechanical energy required by the refrigerator can be thus evaluated thanks to the definition of ideal COP, and assuming T_0 as the environmental temperature (298.15 K) and T as the temperature at which the heat is absorbed from the considered process. Finally, it is assumed that the mechanical energy absorbed by the refrigerator is produced by the same methane-fired combined cycle power plant previously introduced. On the other hand, if the thermal energy is provided to the process, the heat is supplied by means of low-pressure steam produced by a methane-fired boiler, with an energy efficiency η_B of 0.8 [7]. In a different manner, the exergy equivalent of the heat interactions (both removed or provided) can be evaluated based on the definition of the Carnot Factor $\tau_k = 1 - T_0/T_k$ [78], which is based on both the temperatures of the environment T_0 and of the surfaces T_k at which the heat transfer occurs $\dot{Q}_k$. The magnitude and direction of the heat exergy flows depend on values and signs of $\dot{Q}_k$ and τ_k.

Material interactions. The Net equivalent methane analysis does not account for the methane required or saved by the inlet and outlet flows of material streams. On the other hand, exergy analysis accounts for the exergy equivalent of a bulk flow stream as the maximum work extractable from that stream, bringing it from its generic state to the environmental ones in terms of temperature, pressure and chemical composition [78]. Therefore, with respect to the Net equivalent methane method, Exergy analysis allows to write a complete exergy balance for the analyzed system, including all the material and energy streams that cross its boundaries. Neglecting the effects due to magnetism, surface tension, nuclear reactions, change in velocity and elevation, and so on, the exergy equivalent of material streams results for all the analyzed processes as the sum of physical and chemical exergy [81]. *Physical exergy* is defined as the maximum work obtainable bringing the material stream (a mixture of chemical compounds) in thermal and mechanical equilibrium with the environment (i.e. *environmental state*). On the other hand, *chemical exergy* is defined as the maximum work obtainable taking the stream form environmental state to the *dead state*, characterized by the chemical equilibrium with the environmental air. In the evaluation of chemical exergy, R is the universal gas constant (8.314 J mol^{-1}K^{-1}), γ_i is the *activity coefficient* of the *i-th* compound. The specific chemical exergy of the *i-th* pure compound $ex_{ch,i}$ is available for atmosphere compounds, while for fuels it is calculated using the *Van't Hoff box equilibrium model* [69,82,83].

With reference to Table 4, the following indicators are defined to assess the thermodynamic performance of the analyzed processes:

- *Net equivalent methane*. It is equal to the sum of all the mechanical and thermal energy interactions between the process and the environment, expressed by means of equivalent methane $\dot{E}_{CH4}$, as in relation (14). Notice that only work and heat interactions are accounted in such indicator;

$$\dot{E}_{CH\,4} = \sum_i \dot{E}^W_{CH\,4,i} + \sum_j \dot{E}^Q_{CH\,4,j} \tag{14}$$

- *Rational and Functional exergy efficiencies*. Considering all the energy and material interactions that cross boundaries of the analyzed system, rational exergy efficiency $\eta_{ex,R}$, defined by relation (15), is the ratio between the total exergy outputs and the total exergy inputs, representing the amount of exergy destructions $\dot{E}x_D$ occurring inside each analyzed system (i.e. the amount of thermodynamic irreversibilities). Despite its theoretically correct approach, rational exergy efficiency is expected to produce very high numerical values, since the chemical exergy of the treated hydrocarbons are very high compared to their physical exergy contents. To avoid such problem, the functional exergy efficiency $\eta_{ex,F}$ is defined as the ratio between the change in exergy of the treated flows, which is the actual useful product of the system, and the sum of the exogenous exergy requirements of the system. In this way, values of chemical exergy of inlet and outlet streams cancel out, obtaining a more detailed and meaningful performance indicator. More specifically, the numerator of $\eta_{ex,F}$ represents the minimum amount of mechanical work required to separate and to liquefy the natural gas stream, while the denominator represents the amount of mechanical work that must be delivered to the real analyzed process in order to obtain such useful effect.

$$\eta_{ex,R} = \frac{\sum_{OUT} \dot{E}x^{OUT}}{\sum_{IN} \dot{E}x^{IN}} \quad ; \quad \eta_{ex,F} = \frac{\sum_{\mathrm{P}} \dot{E}x^{P}}{\sum_{F} \dot{E}x^{F}} = \frac{\sum_{OUT} \dot{N}_i \left(ex_{ph} + ex_{ch}\right)_i - \sum_{IN} \dot{N}_j \left(ex_{ph} + ex_{ch}\right)_j}{\sum_k \left(\dot{E}x^W_k + \dot{E}x^Q_k\right)} \tag{15}$$

Table 4. Equivalent methane and Exergy of energy/material interactions of the analyzed system.

	Net equivalent methane analysis	**Exergy analysis**
Work interactions (provided / extracted)	$\dot{E}^{W}_{CH4} = \dot{W}/\eta_{CC}$	$\dot{E}x^{W} = W + P \cdot \frac{dV}{dt}$
Heat interactions	Extracted from the process: $\dot{E}^{Q}_{CH4} = \frac{\dot{Q}}{\eta_{II} \cdot \frac{T}{T_o - T} \cdot \eta_{CC}}$ Provided to the process: $\dot{E}^{Q}_{CH4} = \dot{Q}/\eta_{B}$	$\dot{E}x^{Q}_{k} = \dot{Q}_k \cdot \tau \quad ; \quad \tau = \left(1 - \frac{T_0}{T_k}\right)$
Material interactions	-	Physical exergy of mixtures: $ex_{ph,\mathrm{mix}} = \sum_i y_i \cdot \left[(h_i - h_{0,i}) - T_0 \cdot (s_i - s_{0,i})\right]$ Chemical exergy of mixtures: $ex_{ch,mix} = \sum_i (y_i \cdot ex_{ch,i}) + T_0 R \sum_i \left[y_i \ln(\gamma_i y_i)\right]$

4.2. Methods application, results and discussion

Main properties of the natural gas inlet and the LNG and CO_2 outlet material streams are collected in Table 5. Molar enthalpy and entropy are accounted with respect to the reference conditions of the same flows (superscript "°"). Values of physical, chemical and total exergy of such material flows are also reported. As previously introduced, values of chemical exergy are about two orders of magnitude lower with respect to the values of physical exergy for the natural gas and the LNG streams. Moreover, values of chemical exergy of inlet natural gas and outlet LNG are almost equal, since the analyzed systems do not cause a changes in the chemical nature of material flows, but only a change in their thermo-physical properties.

By handling values in Table 5, the minimum amount of work required to separate and to liquefy the natural gas inlet can be derived. The minimum work required to separate the methane and the CO_2 is equal to the difference between the chemical exergy of outlet and inlet flows (2353 kW), while the minimum work required to liquefy the LNG and CO_2 streams is equal to the difference between physical exergy of outlet and inlet flows (6813 kW). The sum of these two values (9166 kW) represent the reference thermodynamic upper limit for the analyzed separation and liquefaction process.

With reference to the analyzed process schemes (Figure 5, Figure 6 and Figure 10), Table 6 collects numerical values for the energy associated to heat and work interactions that cross system boundaries. Mechanical and thermal energy requirements have been calculated using Aspen Hysys® V7.3, except for thermal streams related to heat exchangers where dry ice formation occurs, allowing to close material and energy balances for all the considered processes. Magnitude and direction of the equivalent methane and the exergy associated to all the heat/work interactions are also reported, together with values of Carnot

factor and the temperature of boundaries at which heat transfers occur. Note that the directions of energy, exergy and equivalent methane associated to a same heat flow may be different, depending on the temperature level at which the heat exchanging process occurs, while the directions of exergy and equivalent methane results always the same.

Table 5. Main properties of material flows that cross system boundaries. These properties are constant for all the three analyzed processes.

Property	Symbol	Unit	INLET NG	LNG	CO_2 (l)
Molar enthalpy	h-h°	J/mol	-787,4	-14742,5	-11462,6
Molar entropy	s-s°	J/mol-K	-33,9928	-108,2941	-69,6851
Molar physical exergy	ex_{ph}	J/mol	9347,5	17545,4	9314,0
Molar chemical exergy	ex_{ch}	J/mol	504479,3	830132,5	20185,2
Molar exergy	ex_{tot}	J/mol	513826,8	847677,8	29500,0
Physical exergy	Ex_{ph}	kW	12983	14622	5174
Chemical exergy	Ex_{ch}	kW	700666	691805	11214
Exergy	Ex_{tot}	kW	713648	706426	16388

Table 6. Energy (E), Exergy (Ex) and equivalent methane (E_{CH4}) of heat and work streams for all the analyzed systems. The temperature (T_k) and Carnot factor (τ_k) that characterize the heat transfer processes are also listed.

System	Component	No	Type	E [kW]	T_k [K]	τ_k [-]	Ex [kW]	E_{CH4} [kW]
1. Dual pressure	Natural Gas cooler 1	1	Heat	-2556.2	257.1	-0.160	408.4	1375.0
	HP distillation column	2	Heat	4302.3	298.2	0.000	0.0	0.0
	Natural Gas cooler 2	3	Heat	-7406.4	190.1	-0.569	4212.5	13100.0
	Pump	4	Work	308.4	-	-	308.4	560.0
	LP distillation column	5	Heat	-5171.3	180.7	-0.650	3360.3	10550.0
	Expander	6	Work	-1640.4	-	-	-1640.4	-2985.0
	LNG cooler	7	Heat	-5383.8	107.4	-1.777	9569.0	28650.0
	Total	tot	-	-	-	-	16218.1	51250.0
2. Anti-subl.	Pump	1	Work	124.6	-	-	124.6	226.4
	Antisub. heat exch.	2	Heat	-13194.3	108.2	-1.757	23180.0	70000.0
	LNG cooler	3	Heat	-7023.1	107.5	-1.775	12464.4	37400.0
	Total	tot	-	-	-	-	35769.0	107626.4
3. Hybrid	Natural Gas cooler 1	1	Heat	-2383.9	275.2	-0.083	198.8	659.7
	Pump	2	Work	20.8	-	-	20.8	37.5
	HP distillation column	3	Heat	-8413.5	206.5	-0.444	3731.4	11900.0
	HP distillation column	4	Heat	3043.9	298.2	0.000	0.0	0.0
	Antisub. heat exch.	5	Heat	-5277.0	108.2	-1.757	9270.8	28100.0

LNG cooler	6	Heat	-7022.7	107.5	-1.775	12463.7	37400.0
Total	tot	-	-	-	-	25685.5	78097.2

In order to derive the exergy equivalents of thermal flows, the temperature at which heat exchange occurs must be known: the temperatures of the utilities have been defined starting from the ones of process streams across heat exchangers and assuming as minimum temperature approach 5 K for refrigerants and 10 K for steam. The proposed values are conventionally established by the literature [84]. These procedure has been applied to all heat exchangers that have been assumed as operating in counter-current mode, except for AHEs, namely the ones in which solid phase formation occurs. Moreover, the temperature inside these equipment has been assumed as homogeneous: in this way, the utility temperature has been estimated assuming 5 K as the minimum temperature approach with respect to the minimum temperature achieved on process side. In some cases, zero-cost utilities (like water or air) have been considered, and also the associated energy stream costs have been neglected. In the Dual-pressure process, the heat is released by the HP distillation column at environmental temperature: this heat flow is considered as not recoverable by the exergy analysis (i.e. its exergy content is equal to zero). On the other hand, in the same process a flow of mechanical work easily recoverable is produced by the Expander, and thus it has been considered as a saving of the exergy requirements of the plant.

To better understand the exergy flows that cross system boundaries, Grassmann diagrams [85] have been reported in Figure 13 for the three analyzed processes: grey arrows represent the exergy associated to material streams, while black arrows represent the exergy equivalents of heat and work flows.

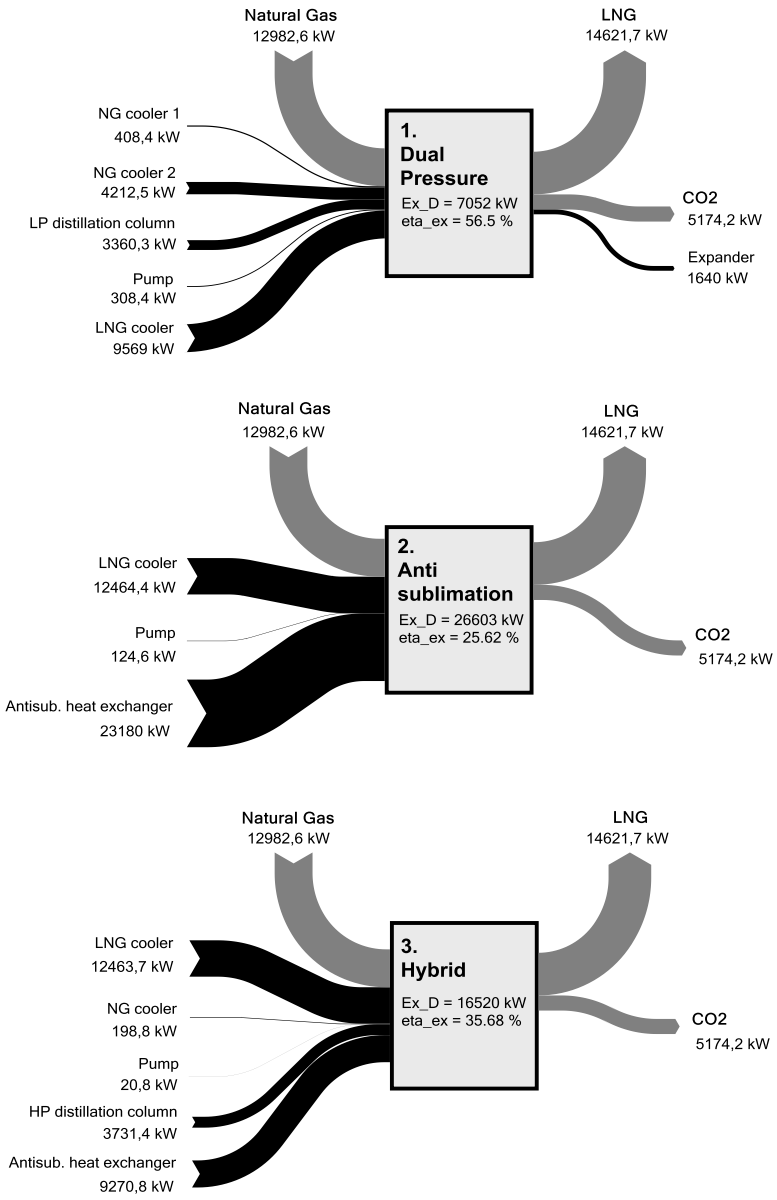

Figure 13. Grassmann diagrams for the analyzed processes. Notice that only values of physical exergy are represented for the streams of Natural Gas, LNG and CO_2.

With reference to Figure 13, the following comments can be made:

- Only the physical exergy of the material streams (Natural Gas, LNG, CO_2) is depicted, since values of chemical exergy of single compounds are not affected by the analyzed processes of separation and liquefaction;
- The numerical differences between all the inlet and outlet flows of the three processes result in the total exergy destructions caused by the systems. As can be inferred from the numerical results collected in Table 7, the Antisublimation process has the lowest thermodynamic performances, followed by the Hybrid and the Dual pressure schemes;
- The Anti sublimation process presents the largest exergy requirements with respect to the other processes: in particular, the Antisublimation heat exchanger rejects large amounts of heat at very

low temperatures, resulting in such high exergy inflows. Moreover, a critical component of all the three analyzed processes is the LNG cooler: the heat released by this component is numerically lower with respect to its exergy equivalent, since the heat transfer is characterized by the lowest temperatures of the whole process;

- Exergy associated to work absorbed by pumps is numerically negligible with respect to the exergy equivalents of heat flows. However, the work produced by the Expander in the Dual Pressure process results as non-negligible (1640 kW) with respect to the other exergy flows.

Table 7. Results of the net equivalent methane and the exergy analyses: consumption of equivalent methane (E_{CH4}) exergy destructions (Ex_D), rational and functional exergy efficiencies ($\eta_{ex,R}$, $\eta_{ex,F}$).

	E_{CH4} [kW]	Ex_D [kW]	$\eta_{ex,r}$ [%]	$\eta_{ex,f}$ [%]
1. Dual pressure	51250	7052	99,04%	56,52%
2. Anti-subl.	107626	26603	96,45%	25,62%
3. Hybrid	78097	16520	97,77%	35,68%

For the three analyzed processes, results of Net equivalent methane and Exergy analyses are reported in Table 7 in terms of consumption of equivalent methane (E_{CH4}), exergy destructions (Ex_D), rational and functional exergy efficiencies ($\eta_{ex,R}$, $\eta_{ex,F}$). Based on these results, the following comments can be made:

- Since the three process layouts have been simulated assuming the same material flows at battery limits, the key factor in determining the efficiency classification for exergy analysis is represented by the contribution of mechanical and thermal streams, as well as for net equivalent methane analysis;
- The thermodynamic performance ranking of the three analyzed process is the same with energy and exergy analyses. From a purely thermodynamic viewpoint, the Dual Pressure scheme (scheme 1, Figure 5) is the most efficient process, while the Antisublimation (scheme 2, Figure 6) is less efficient. The Hybrid solution (scheme 3, Figure 10) lies in the middle between the other two processes;
- While energy analysis provides absolute values for the methane required to sustain each process, exergy analysis provides a value for their efficiencies, enabling to quantify how much each process is far from the ideal thermodynamic reference process. Therefore, even if the thermodynamic performance ranking of the three analyzed process is the same according to energy and exergy analyses, the latter provides more useful information and thus it should be preferred;
- The Dual Pressure process results more efficient because distillation occurs following a temperature profile along the distillation column. The Anti-sublimation process, on the contrary, is more energy intensive because the stream is globally cooled down at the required temperature. Moreover, distillation involves the latent heat of vaporization, whose value is lower than the sublimation one. Since the hybrid layout combines both the purification solutions, its thermodynamic performances are therefore placed in the middle between the two other processes;
- Values of rational and functional exergy efficiencies rank the processes in the same way. As expected, and with reference to relation (15), values of rational exergy efficiencies $\eta_{ex,R}$ result

numerically similar and close to 100%: this is due to the effects of the chemical exergy of the inlet and outlet flows. On the other hand, the definition of functional exergy efficiency results in more meaningful values, and it is then recommended;

5. Conclusion

In order to liquefy an acid gas stream, characterized by a high CO_2 level, sweetening is required to meet the purity specification (50 ppm for CO_2) of the final product. The possible synergy between the average thermal level at which cryogenic purifications occur and the operating conditions required for LNG production has suggested to evaluate and compare the efficiency of three types of cryogenic purification solutions combined with LNG production. In particular, a dual pressure distillation process, an anti-sublimation on heat exchanger and a hybrid process configuration have been considered for this purpose. The three process schemes have been compared using two different approaches both able to harmonize the different nature of energy streams. The net equivalent methane analysis accounts for the amount of methane required to supply the overall process energy demands through specific processes assumed as reference. On the other hand, the exergy analysis evaluates the exergy efficiency of each process scheme through a thermodynamically rigorous approach, converting energy and material flows into their relative exergy equivalents.

The results obtained with both the methodologies show the same trend: the process scheme which achieves the natural gas purification involving a distillation unit results the less energy intensive. This is mainly due to the spatial temperature profile typical of a distillation column, that allow to optimize the use of energy inside the process because purification occurs together with an evolving temperature profile. On the other hand, in the anti-sublimation process the purification is performed inside a heat exchanger where the utility is at constant temperature. This fact does not allow to keep a parallelism in the two curves of the heat exchanger due to pinch limitations. It is of interest, in this way, to consider the coupling of low-temperature distillation technologies (or analogous processes that allow to better distribute the temperature profile) to the production of LNG, in order to allow a better management of process energy. Based on the obtained results, it is possible to notice that the combination of energy and exergy analyses extended to complex systems, such as for low-temperature purification and natural gas liquefaction, can be an effective tool to better define pathways and possibilities to improve the use of energy for LNG production considering not only the liquefaction process, but also the purification step that is required to provide a feed gas at the purity level required for the liquefaction unit. This method allows to better asses the definition of complete process schemes, including interactions between different process operation. Moreover, these analyses are applied to the study of innovative gas purification technologies for the exploitation of CO_2-rich gas reserves, a context where a proper use of energy is compulsory in order to minimize energy losses, external utilities dependence, and optimize the use of valuable energy to reduce energy expenses that might negatively impact the possibility of developing low-quality gas reserves.

6. Nomenclature

Symbol	Quantity	Unit
COP	Coefficient of Performance	[-]
Cp	Specific Heat at Constant Pressure	J mol^{-1} K^{-1}
Ex	Exergy	kJ
$\dot{E}_x$	Exergy rate	kW
F	Feed Molar Flow	kmol h^{-1}
$\dot{H}$	Enthalpy rate	kW
LHV	Lower Heating Value	MJ kg^{-1}
$\dot{m}$	Mass Flow	kg s^{-1}
$\dot{n}$	Molar Flow	kmol h^{-1}
P	Pressure	bar
$\dot{Q}$	Duty	kW
R	Ideal Gas Constant	J mol^{-1} K^{-1}
T	Temperature	K
t	Time	s
V	Vapor Flow	kmol h^{-1}
V	Volume in Equation (21)	m^3
W	Electric Power	kW
x	Liquid Phase Mole Fraction	mol mol^{-1}
y	Vapor Phase Mole Fraction	mol mol^{-1}
Δh	Latent Heat	kJ $kmol^{-1}$
η	Efficiency	[-]
τ	Carnot Factor	[-]
γ	Activity Coefficient	[-]

7. Acronyms

AAD%	Absolute Average Deviation %
AHE	Anti-sublimation Heat Exchanger
BFD	Block Flow Diagram
CCS	Carbon Capture and Storage

EOR	Enhanced Oil Reovery
EoS	Equation of State
HP	High Pressure
IEA	International Energy Agency
JT	Joule-Thomson
L	Liquid
LNG	Liquefied Natural Gas
LP	Low Pressure
MDEA	Methyl Di-Ethanol Amine
mol	Molar Basis
NG	Natural Gas
RHE	Recovery Heat Exchanger
S	Solid
SAP	Standard Ambient Pressure
SAT	Standard Ambient Temperature
SLE	Solid-Liquid-Equilibrium
SLVE	Solid-Liquid-Vapor-Equilibrium
SRK	Soave-Redlich-Kwong
SVE	Solid-Vapor-Equilibrium
V	Vapor
VLE	Vapor-Liquid-Equilibrium

Subscripts

B	Boiler
CC	Combined Cycle
ch	Chemical
D	Destroyed
el	Electric
F	Cold
gen	Generated

i	Generic Component
id	Ideal
IN	Inlet
j	Generic Index
k	Generic Index
kn	Kinetic
mix	Mixture
OUT	Outlet
p	Generic Index
ph	Physical
pt	Potential
q	Generic Index
rev	Reversible
rif	Reference State
tri	Triple Point
II	Second Principle of Thermodynamics
0	Reference State for Exergy Analysis

Superscripts

cond	Condensation
ev	Evaporation
G	Gas
IN	Inlet
$\dot{m}$	Exergy Contribution Related to Material Flows
$\dot{Q}$	Exergy Contribution Related to Heat
sub	Sublimation
$\dot{W}$	Exergy Contribution Related to Mechanical Work

8. References

[1] Carroll J, Foster J. New Challenges & Solutions in Designing Large Sour Gas Projects. 2008.

[2] Bagirov LA, Imaev SZ, Borisov VE. R&D Technologies for Acid Gases Extraction from Natural Gases. SPE/IATMI Asia Pacific Oil Gas Conf. Exhib. Nusa Dua, Indones., Society of Petroleum Engineers; 2015.

[3] Burgers WFJ, Northrop PS, Kheshgi HS, Valencia J a. Worldwide development potential for sour gas. Energy Procedia 2011;4:2178–84.

[4] Rojey A, Jaffret C. Natural gas: production, processing, transport. Editions Technip; 1997.

[5] Parker ME, Northrop S, Valencia J a., Foglesong RE, Duncan WT. CO2 management at ExxonMobil's LaBarge field, Wyoming, USA. Energy Procedia 2011;4:5455–70.

[6] Kelley BT, Valencia JA, Northrop PS, Mart CJ. Controlled Freeze Zone™ for developing sour gas reserves. Energy Procedia 2011;4:824–9.

[7] Langè S, Pellegrini LA, Vergani P, Lo Savio M. Energy and Economic Analysis of a New Low-Temperature Distillation Process for the Upgrading of High-CO2 Content Natural Gas Streams. Ind Eng Chem Res 2015;54:9770–82.

[8] International Energy Agency. World Energy Outlook 2015. 2015.

[9] Bp. BP Energy Outlook 2035. 2014.

[10] Haut RC, Denton, R.D. Thomas E. Development and application of the controlled-freeze-zone process. SPE Prod Eng 1989;4:265–71.

[11] Northrop PS, Valencia JA. The CFZ™ process: a cryogenic method for handling high-CO2 and H2S gas reserves and facilitating geosequestration of CO2 and acid gases. Energy Procedia 2009;1:171–7.

[12] Valencia JA, Denton RD. Method and apparatus for separating carbon dioxide and other acid gases from methane by the use of distillation and a controlled freezing zone. U.S.4533372, 1985.

[13] Valencia JA, Victory DJ. Method and apparatus for cryogenic separation of carbon dioxide and other acid gases from methane. U.S.4923493, 1990.

[14] Valencia JA, Victory DJ. Bubble cap tray for melting solids and method for using same. U.S.5265428, 1993.

[15] Amin R, Jackson AT, Kennaird T. The Cryocell: an advanced gas sweetening technology. Int. Pet. Technol. Conf. Doha, Quatar, International Petroleum Technology Conference; 2005.

[16] Hart A, Gnanendran N. Cryogenic CO2 capture in natural gas. Energy Procedia 2009;1:697–706. doi:10.1016/j.egypro.2009.01.092.

[17] Cryo Pur n.d.

[18] Clodic D, Younes M. A new method for CO2 capture: frosting CO2 at atmospheric pressure. Sixth Int. Conf. Greenh. Gas Control Technol. GHGT6, Kyoto, Japan, 2002, p. 155–60.

[19] Xiong X, Lin W, Gu A. Integration of CO2 cryogenic removal with a natural gas pressurized liquefaction process using gas expansion refrigeration. Energy 2015;93:1–9.

[20] Holmes AS, Ryan JM. Distillative separation of carbon dioxide from light hydrocarbons. U.S.4350511, 1982.

[21] Holmes AS, Ryan JM. Cryogenic distillative separation of acid gases from methane. U.S.4318723, 1982.

[22] Holmes AS, Price BC, Ryan JM, Styring RE. Pilot tests prove out cryogenic acid-gas/hydrocarbon separation processes. Oil Gas J 1983;81.

[23] Lallemand F, Perdu G, Prosernat LN, Total CW, Magne-drisch J, Gonnard S, et al. Extending the treatment of highly sour gases : cryogenic distillation 2014:1–8.

[24] Lallemand F, Lecomte F, Streicher C. Highly sour gas processing: H2S bulk removal with the sprex process. Int. Pet. Technol. Conf. Doha, Qatar, International Petroleum Technology Conference; 2005.

[25] Pellegrini LA. Process for the removal of CO2 from acid gas. W.O. 2014/054945A2, 2014.

[26] Dauber F, Span R. Modelling liquefied-natural-gas processes using highly accurate property models. Appl Energy 2012;97:822–7. doi:10.1016/j.apenergy.2011.11.045.

[27] Lim W, Choi K, Moon I. Current Status and Perspectives of Liquefied Natural Gas (LNG) Plant Design. Ind Eng Chem Res 2013;52:3065–88.

[28] Tamura I, Tanaka T, Kagajo T, Kuwabara S, Yoshioka T, Nagata T, et al. Life cycle CO 2 analysis of LNG and city gas. Appl Energy 2001;68:301–19.

[29] Arteconi A, Brandoni C, Evangelista D, Polonara F. Life-cycle greenhouse gas analysis of LNG as a heavy vehicle fuel in Europe. Appl Energy 2010;87:2005–13. doi:10.1016/j.apenergy.2009.11.012.

[30] Kumar S, Kwon H, Choi K, Lim W, Hyun J, Tak K, et al. LNG : An eco-friendly cryogenic fuel for sustainable development. Appl Energy 2011;88:4264–73. doi:10.1016/j.apenergy.2011.06.035.

[31] Hisazumi Y, Yamasaki Y, Sugiyama S. Proposal for a high e • ciency LNG power- generation system utilizing waste heat from the combined cycle 1. Appl Energy 1998;60:169–82.

[32] Wood DA. A review and outlook for the global LNG trade. J Nat Gas Sci Eng 2012;9:16–27.

[33] Aspelund A, Gundersen T. A liquefied energy chain for transport and utilization of natural gas for power production with CO 2 capture and storage – Part 1. Appl Energy 2009;86:781–92. doi:10.1016/j.apenergy.2008.10.010.

[34] Aspelund A, Gundersen T. A liquefied energy chain for transport and utilization of natural gas for power production with CO 2 capture and storage – Part 2 : The offshore and the onshore processes. Appl Energy 2009;86:793–804. doi:10.1016/j.apenergy.2008.10.022.

[35] Aspelund A, Gundersen T. A liquefied energy chain for transport and utilization of natural gas for power production with CO 2 capture and storage – Part 4 : Sensitivity analysis of transport pressures and benchmarking with conventional technology for gas transport. Appl Energy 2009;86:815–25. doi:10.1016/j.apenergy.2008.10.021.

[36] Aspelund A, Tveit SP, Gundersen T. A liquefied energy chain for transport and utilization of natural gas for power production with CO 2 capture and storage – Part 3 : The combined carrier and onshore

storage. Appl Energy 2009;86:805–14. doi:10.1016/j.apenergy.2008.10.023.

[37] Li Y, Wang X, Ding Y. An optimal design methodology for large-scale gas liquefaction. Appl Energy 2012;99:484–90. doi:10.1016/j.apenergy.2012.04.040.

[38] Kaneko, K. I., Ohtani, K., Tsujikawa, Y., Fujii S. Utilization of the cryogenic exergy of LNG by a mirror gas-turbine. Appl Energy 2004;79:355–69.

[39] Shariq M, Lee S, Rangaiah GP, Lee M. Knowledge based decision making method for the selection of mixed refrigerant systems for energy efficient LNG processes. Appl Energy 2013;111:1018–31. doi:10.1016/j.apenergy.2013.06.010.

[40] Chang H-M. A thermodynamic review of cryogenic refrigeration cycles for liquefaction of natural gas. Cryogenics (Guildf) 2015;72:127–47.

[41] De Guido G, Langè S, Pellegrini LA. Refrigeration Cycles in Low-Temperature Distillation Processes for the Purification of Natural Gas. J Nat Gas Sci Eng 2015.

[42] Aspen HYSYS® V7.3. Thermodynamics COM interface reference guide; unit operations guide, in: AspenONE V7.3 documentation. Burlington, MA: 2011.

[43] Soave G. Equilibrium constants from a modified Redlich-Kwong equation of state. Chem Eng Sci 1972;27:1197–203. doi:10.1016/0009-2509(72)80096-4.

[44] De Guido G, Langè S, Moioli S, Pellegrini L a. Thermodynamic method for the prediction of solid CO2 formation from multicomponent mixtures. Process Saf Environ Prot 2014;92:70–9.

[45] Donnelly HG, Katz DL. Phase equilibria in the carbon dioxide–methane system. Ind Eng Chem 1954;46:511–7.

[46] Davis JA, Rodewald N, Kurata F. Solid- liquid- vapor phase behavior of the methane- carbon dioxide system. AIChE J 1962;8:537–9.

[47] Eggeman T, Chafin S. Beware the pitfalls of CO2 freezing prediction. Chem Eng Prog 2005;101:39–44.

[48] Riva M, Campestrini M, Toubassy J, Clodic D, Stringari P. Solid–liquid–vapor equilibrium models for cryogenic biogas upgrading. Ind Eng Chem Res 2014;53:17506–14.

[49] Stringari P, Campestrini M, Coquelet C, Arpentinier P. An equation of state for solid–liquid–vapor equilibrium applied to gas processing and natural gas liquefaction. Fluid Phase Equilib 2014;362:258–67.

[50] Van Konynenburg PH, Scott RL. Critical lines and phase equilibria in binary van der Waals mixtures. Philos Trans R Soc London A Math Phys Eng Sci 1980;298:495–540.

[51] Berstad D, Anantharaman R, Nekså P. Low-temperature CO2 capture technologies - Applications and potential. Int J Refrig 2013;36:1403–16. doi:10.1016/j.ijrefrig.2013.03.017.

[52] International Energy Agency. World energy outlook. vol. 23. 2008. doi:10.1049/ep.1977.0180.

[53] Poling BE, Prausnitz JM, O'connell JP. The properties of gases and liquids. vol. 5. McGraw-Hill New

York; 2001.

[54] Green, DW, Perry R. Perry's Chemical Engineers' Handbook. 7 ediction. McGraw-hill New York; 1999.

[55] Green DW. Perry's chemical engineers' handbook. vol. 796. McGraw-hill New York; 2008.

[56] Giauque WF, Egan CJ. Carbon dioxide. The heat capacity and vapor pressure of the solid. The heat of sublimation. Thermodynamic and spectroscopic values of the entropy. J Chem Phys 1937;5:45–54.

[57] NIST - National Institute of Standards and Technology n.d.

[58] Chemical Engineering Research Information Center n.d.

[59] Air Liquide Encyclopedia n.d. http://encyclopedia.airliquide.com/encyclopedia.asp.

[60] Naletov VA, Lukyanov VL, Kulov NN, Naletov AY, Glebov MB. An experimental study of desublimation of carbon dioxide from a gas mixture. Theor Found Chem Eng 2014;48:312–9.

[61] Naletov VA, Gordeev LS, Glebov MB, Naletov AY. Mathematical modeling of desublimation of carbon dioxide from flue gases of heat power systems. Theor Found Chem Eng 2014;48:27–33.

[62] Song CF, Kitamura Y, Li SH, Jiang WZ. Analysis of CO2 frost formation properties in cryogenic capture process. Int J Greenh Gas Control 2013;13:26–33.

[63] Clodic D, Paris M De, Hitti R El, Younes M, Bill A, Environment AP. CO2 capture by anti-sublimation Thermo-economic process evaluation. 4Th Annu Conf Carbon Capture Sequestration, Alexandria, USA 2005:1–11.

[64] Clodic D, Younes M. Method and system for extracting carbon dioxide by anti-sublimation for storage thereof. U.S.7073348, 2006.

[65] Hees WG, Monroe CM. Method and system for extracting carbon dioxide by anti-sublimation at raised pressure. U.S.8163070, 2012.

[66] Shchelkunov VN, Rudenko NZ, Shostak Y V, Dolganin VI. Surface desublimation of carbon dioxide from binary gas mixtures. J Eng Phys 1986;51:1432–5.

[67] Pellegrini LA, Langè S, Baccanelli M, De Guido G. Techno-Economic Analysis of LNG Production Using Cryogenic Vs Conventional Techniques for Natural Gas Purification. Offshore Mediterr. Conf. Exhib. Ravenna, Italy, 2015.

[68] Kotas TJ. The exergy method of thermal plant analysis. Paragon Pu. 2012.

[69] Bejan A. Advanced Engineering Thermodynamics. John Wiley & Sons; 2006.

[70] Bejan A. Fundamentals of exergy analysis, entropy generation minimization, and the generation of flow architecture. Int J Energy Res 2002;26:0–43.

[71] Moran MJ, Sciubba E. Exergy analysis: principles and practice. ASME Trans J Eng Gas Turbines Power 1994;116:285–90.

[72] Moran MJ, Shapiro HN, Boettner DD, Bailey MB. Fundamentals of engineering thermodynamics. John Wiley & Sons; 2010.

[73] Keshavarzian S, Gardumi F, Rocco M, Colombo E. Off-Design Modeling of Natural Gas Combined Cycle Power Plants: An Order Reduction by Means of Thermoeconomic Input–Output Analysis. Entropy 2016;18:71. doi:10.3390/e18030071.

[74] Colombo E, Rocco M V, Toro C, Sciubba E. An exergy-based approach to the joint economic and environmental impact assessment of possible photovoltaic scenarios: A case study at a regional level in Italy. Ecol Modell 2015;318:64–74. doi:10.1016/j.ecolmodel.2014.11.006.

[75] Orsi F, Muratori M, Rocco M, Colombo E, Rizzoni G. A multi-dimensional well-to-wheels analysis of passenger vehicles in different regions: Primary energy consumption, CO 2 emissions, and economic cost. Appl Energy 2016;169:197–209.

[76] Moran MJ, Shapiro HN. Fundamentals of Engineering Thermodynamics. Wiley; 2006.

[77] Kehlhofer R, Rukes B, Hannemann F, Stirnimann F. Combined-cycle gas & steam turbine power plants. Tulsa, OK, USA: Pennwell Books; 2009.

[78] Kotas TJ. The exergy method of thermal plant analysis. Butterworths; 1985.

[79] Cengel YA, Boles MA, Kanoğlu M. Thermodynamics: an engineering approach. vol. 5. McGraw-Hill New York; 2002.

[80] Kanoğlu M. Exergy analysis of multistage cascade refrigeration cycle used for natural gas liquefaction. Int J Energy Res 2002;26:763–74.

[81] Querol E, Gonzalez-Regueral B, Perez-Benedito JL. Practical approach to exergy and thermoeconomic analyses of industrial processes. Springer Science & Business Media; 2012.

[82] Kotas TJ. The exergy method of thermal plant analysis. Malabar: Elsevier; 2013.

[83] 1996_Bejan,Tsatsaronis,Moran_Thermal Design and Optimization.pdf n.d.

[84] Turton R, Bailie RC, Whiting WB, Shaeiwitz JA. Analysis, synthesis and design of chemical processes. Prentice Hall; 2003.

[85] Graveland a. JGG, Gisolf E. Exergy analysis: An efficient tool for process optimization and understanding. Demonstrated on the vinyl-chloride plant of Akzo Nobel. Comput Chem Eng 1998;22:S545–52. doi:10.1016/S0098-1354(98)00099-4.